PAPER

Non-linear magnetohydrodynamic simulations of edge localised mode triggering via vertical position oscillations in ITER

IOP Publishing | International Atomic Energy Agency Nuclear Fusion

Nucl. Fusion **58** (2018) 096018 (12pp) https://doi.org/10.1088/1741-4326/aace0e

Non-linear magnetohydrodynamic simulations of edge localised mode triggering via vertical position oscillations in ITER

F.J. Artola[1,5], G.T.A. Huijsmans[2,3], M. Hoelzl[4], P. Beyer[1], A. Loarte[5] and Y. Gribov[5]

[1] Aix-Marseille Université, CNRS, PIIM UMR 7345, 13397 Marseille, France
[2] CEA, IRFM, F-13108 St. Paul-lez-Durance cedex, France
[3] Eindhoven University of Technology, Eindhoven, Netherlands
[4] Max Planck Institute for Plasmaphysics, Boltzmannstr. 2, 85748 Garching, Germany
[5] ITER Organization, Route de Vinon sur Verdon, 13067 St Paul Lez Durance Cedex, France

E-mail: javier.artola@iter.org

Received 23 March 2018, revised 6 June 2018
Accepted for publication 21 June 2018
Published 10 July 2018

Abstract

Magnetic triggering of edge localized modes (ELMs) in Ohmic H-mode plasmas was first reported in the TCV tokamak (Degeling *et al* 2003 *Plasma Phys. Control. Fusion* **45** 1637). This method, showing reliable locking of the ELM frequency to an imposed axisymmetric vertical plasma oscillation, was also demonstrated in the ITER-relevant type-I ELM regime in ASDEX Upgrade (Lang *et al* 2004 *Plasma Phys. Control. Fusion* **46** L31) and JET (de la Luna *et al* 2015 *Nucl. Fusion* **56** 026001). However, the mechanisms of the ELM triggering due to a vertical motion has not been studied extensively. The non-linear reduced MHD code JOREK-STARWALL has been extended for 3D free-boundary computations (Hölzl *et al* 2012 *J. Phys.: Conf. Ser.* **401** 012010), which has allowed us to simulate for the first time realistic vertical oscillations together with ELM simulations in a single consistent scheme. Our simulations demonstrate that stable plasmas can be destabilized by the application of a vertical oscillation for ITER. During the vertical motion, a toroidal current is induced in the pedestal. The origin of this current is analysed in detail with the use of simulations and a simple analytical model, revealing that it arises from the compression of the plasma cross section due to its motion through an inhomogeneous magnetic field. Lower pedestal currents between ELMs require bigger vertical displacements to destabilize ELMs, which directly points towards the increased edge current as the ELM driving mechanism. Finally the ELM triggering shows a very weak dependence on the plasma velocity for ITER in agreement with experiments.

Keywords: ELM, ITER, vertical oscillations, non-linear MHD simulations

(Some figures may appear in colour only in the online journal)

1. Introduction

Magnetic triggering of edge localized modes (ELMs) in Ohmic H-mode plasmas was first reported in the TCV tokamak [1]. The experiments showed that imposing a vertical plasma oscillation using poloidal field coils (PF coils), leads to a reliable locking of the ELM frequency to the vertical oscillation frequency. These vertical oscillations often called 'vertical kicks' or 'vertical jogs' were also used for ELM frequency control in the ITER-relevant type-I ELM regime in ASDEX Upgrade [2] and JET [3] tokamaks. This technique can play an important role in controlling the impurity content

of the plasma and the energy released per ELM. For ITER, vertical oscillations are considered as a back-up technique [5] for the initial non-active operation up to half current and half magnetic field (7.5 MA, 2.65 T) to supplement the baseline ELM control scheme (resonant magnetic perturbations by in-vessel coils) as its application is developed.

Linear stability studies were performed for vertical position oscillation simulations for JET [3] and ITER [6]. These studies concluded that the main destabilizing factor was an increase of edge current produced by the oscillations, which is known to destabilize peeling–ballooning modes [7] . However the authors of [8] argued that for the AUG case, ELMs were destabilized when the edge current was decreasing and therefore, ELMs could be triggered by other more subtle factors such as the change in plasma shape or in pressure gradient. The main goal of this work is to clarify which is the determining factor for the ELM destabilization through non-linear simulations and as well, to provide an understanding of the current induction during the plasma motion in ITER plasmas. Our research is performed by using the code couple JOREK-STARWALL [4, 9, 10] as it allows 3D MHD non-linear simulations with free-boundary conditions. A 3D thin resistive wall is available in JOREK-STARWALL as well. To perform the studies in this paper we have included realistic PF and in-vessel coils which take into account all the mutual inductances of the system. All these features allow us to simulate for the first time realistic vertical oscillations together with non-linear MHD ELM triggering simulations in a consistent single scheme.

The paper is organized as follows, in section 2 we investigate the physics of the edge current induction during the plasma vertical motion, where we show analytical results and then we present simulations of both a simplified plasma and a realistic ITER plasma. In section 3 we analyse the non-linear stability of an ITER plasma during a vertical oscillation and we investigate the main causes of ELM destabilization. In this work the destabilization of peeling–ballooning modes is shown up to the non-linear saturation phase and therefore the study of the non-linear dynamics related with ELM crashes and transient outbursts is left for future work. Finally we present our conclusions in section 4.

2. Understanding the axisymmetric induction of edge currents during vertical oscillations

The authors of [3] and [6] concluded that the mechanism underlying ELM triggering was an increase of the edge toroidal current driving the plasma into the unstable MHD peeling–ballooning regime. The induction of edge toroidal current was mainly attributed to a fast reduction of the plasma volume due to the vertical motion through an inhomogeneous magnetic field. Here we investigate this effect analytically in the frame of an MHD model and we show simulations of both a simple elongated plasma and a realistic ITER 7.5 MA/2.65 T plasma.

In the following we aim to give some analytical insights into the current induction in a moving plasma. This effect can be understood by analysing the MHD equation for the poloidal flux ψ[6]

$$\frac{\partial \psi}{\partial t} + \mathbf{v}\cdot\boldsymbol{\nabla}\psi = \eta J_\phi \tag{1}$$

where t, $\mathbf{v}$, η, J_ϕ are respectively time, velocity, resistivity and toroidal current density. By separating the poloidal flux into a contribution of the plasma plus an external contribution ($\psi = \psi_\mathrm{p} + \psi_\mathrm{ext}$) and using the convective time derivative ($\mathrm{d}/\mathrm{d}t \equiv \partial_t + \mathbf{v}\cdot\boldsymbol{\nabla}$) equation (1) becomes

$$\frac{\mathrm{d}\psi_\mathrm{p}}{\mathrm{d}t} = -\frac{\partial \psi_\mathrm{ext}}{\partial t} - \mathbf{v}\cdot\boldsymbol{\nabla}\psi_\mathrm{ext} + \eta J_\phi. \tag{2}$$

In the reference frame of the plasma (i.e. following a flux surface) we find that

$$\delta\psi_\mathrm{p} \approx -\delta\psi_\mathrm{ext} + \eta J_\phi \delta t \tag{3}$$

where $\delta\psi_\mathrm{ext} \approx \delta\psi_\mathrm{ext}(\mathbf{r}_0) + \delta\mathbf{r}\cdot\boldsymbol{\nabla}\psi_\mathrm{ext}$ and $\delta\mathbf{r}$ is the displacement of the flux surface. For an axisymmetric case, the plasma contribution to the poloidal flux can be written in terms of the plasma current

$$\psi_\mathrm{p}(R,Z) = \mu_0 \int J_\phi(R',Z')G(R,Z,R',Z')\mathrm{d}R'\mathrm{d}Z' \tag{4}$$

where $G(R,Z,R',Z')$ is a Green's function given by [11]. The latter integral can be analytically calculated for a cylindrical plasma with a spatially constant current density $J_\phi(t)$ going from the radius r_0 to the plasma edge, which is given by $a(t) \equiv r_0 + w_r(t)$ (see figure 1(*a*)). With these assumptions the plasma poloidal flux is

$$\psi_\mathrm{p}(a,t) \approx \psi_\mathrm{p}(r_0) - B_\theta(r_0)R_0 w_r(t) - \frac{\mu_0}{4\pi}R_0 I_\phi^{w_r}(t) \tag{5}$$

where $I_\phi^{w_r}(t) = 2\pi r_0 w_r(t) J_\phi(t)$ is the total toroidal current contained in the edge region $r \in [r_0, a(t)]$ and we have also assumed that $w_r/r_0 \ll 1$. If we assume now that during the plasma motion the plasma moves rigidly without any change in the region $r \leqslant r_0$, equation (3) becomes

$$\delta I_\phi^{w_r} = \frac{4\pi}{\mu_0 R_0}\left[\delta\psi_\mathrm{ext}(a) - B_\theta(r_0)R_0\delta w_r - \eta J_\phi \delta t\right] \tag{6}$$

and the change of current density is

$$\delta J_\phi = \frac{1}{2\pi r_0 w_r}\left(\delta I_\phi^{w_r} - I_\phi^{w_r}\frac{\delta w_r}{w_r}\right). \tag{7}$$

From equations (6) and (7) we can extract the following conclusions:

- The total induced current $\delta I_\phi^{w_r}$ only depends on the speed of the motion (δt) through the resistive decay term, which can be considered to be small. Therefore there is no velocity dependence for an ideal conductor.
- The total induced current $\delta I_\phi^{w_r}$ is induced by 3 mechanisms.

[6] Here $\psi \equiv R_0 A_\phi$ where R_0 is the major radius and A_ϕ is the toroidal component of the magnetic vector potential.

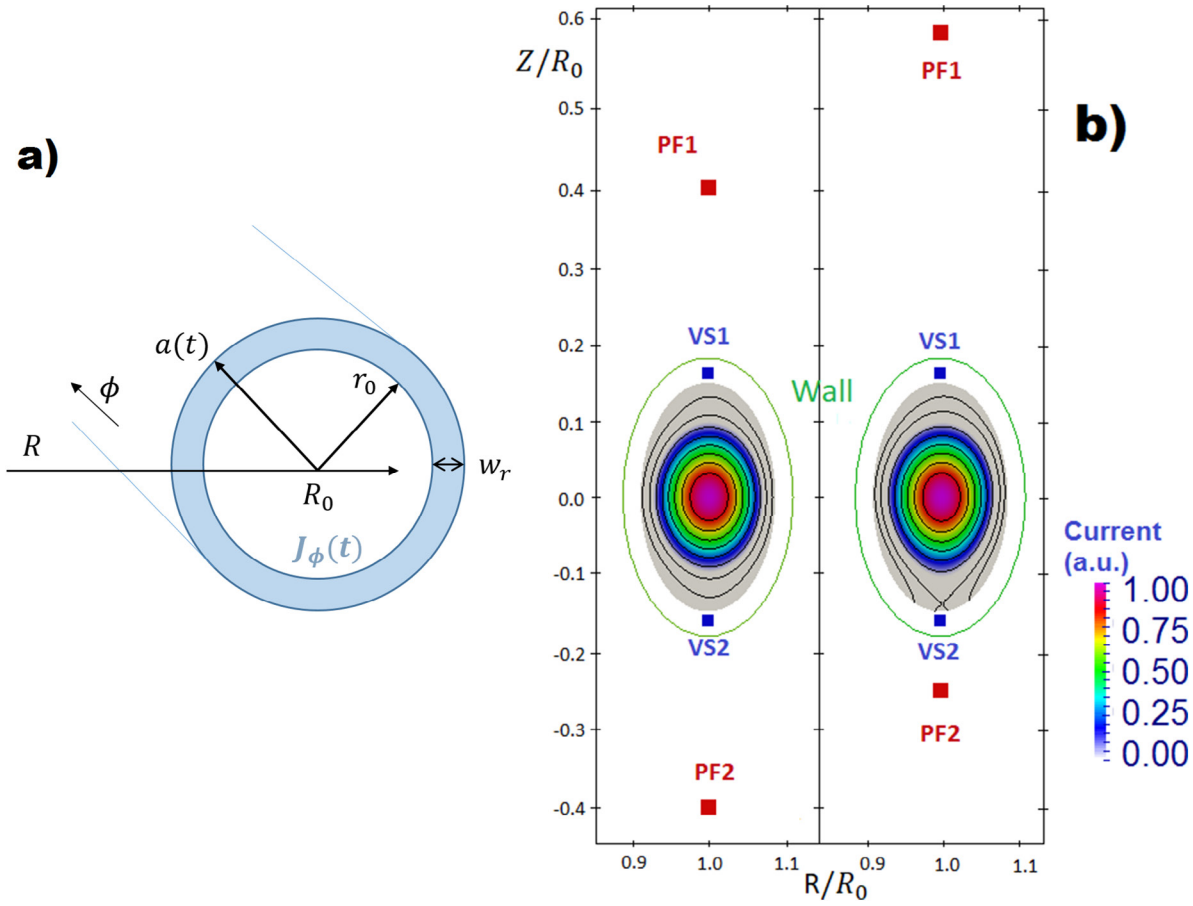

Figure 1. (*a*) Graphical representation of the cylindrical model used for the current induction analytical calculation. (*b*) The two different equilibrium configurations used for the simple plasma simulation cases.

1. Due to a local change in external flux $\delta\psi_{\text{ext}}(a_0)$ (i.e. produced by time variation of currents in PF coils or walls).
2. Due to the motion of the plasma through an inhomogeneous static magnetic field $\delta\mathbf{r}\cdot\nabla\psi_{\text{ext}}$. For this effect, a gradient of external flux is required and plasma deformation also plays an important role through $\delta\mathbf{r}$.
3. Due to plasma compression or expansion (δw_r).

- The variation of current density δJ_ϕ is inversely proportional to the radial width (w_r). This width could be approximated as the skin depth $w_r \sim \sqrt{\eta/(\pi\mu_0 f)}$, where f is the oscillation frequency.
- δJ_ϕ can be produced by two effects

1. An increase in total current in the region of induction ($\delta I_\phi^{w_r}$).
2. A change in the width of the region of induction δw_r (redistribution of current).

2.1. Simple elongated plasma

In the following, we present the case of a simple elongated pressure-less plasma ($\beta_p \ll 1$) that vertically oscillates for 2 different PF coil configurations. For both cases (figure 1(*b*)) the inverse aspect ratio ($\epsilon = 0.07$), the elongation ($\kappa = 1.4$), the ratio between wall and plasma radius ($b_w/a = 1.6$), the plasma size, position and total toroidal current are the same. Besides the 2 PF coils located moderately far from the plasma (PF1, PF2) that provide its elongation, we have also included 2 coils (VS1, VS2)[7] in which currents oscillate in a sinusoidal form and which are located close to the plasma. The latter are used to vary the plasma position over time. These simulations were performed with JOREK-STARWALL using the reduced MHD model presented on [9]. The used grid has a polar structure formed by 2200 bicubic Bezier elements, the maximum Lundquist number is $\sim 10^7$ and the magnetic Prandtl number is $\sim$20. We use a temperature dependent resistivity ($\eta \propto T^{-3/2}$) for these simulations, where the ratio between the vertical oscillation period and the plasma resistive time varies from 10^{-3} at the plasma core up to 10 at the plasma edge. This means that the plasma behaves as an ideal conductor in the plasma core and it transitions continuously to a very resistive plasma at the edge region. The ratio between wall and plasma core resistivity is taken to be 10. The perpendicular particle diffusivity and thermal conductivity are neglected for this study.

2.1.1. Symmetric PF coils. The first PF coil configuration respects vertical symmetry with respect to the plasma magnetic axis (figure 1(*b*)) and the coils (PF1/PF2) have currents

[7] In what follows we will use the name vertical stabilization (VS) coils for the coils in which currents vary over time.

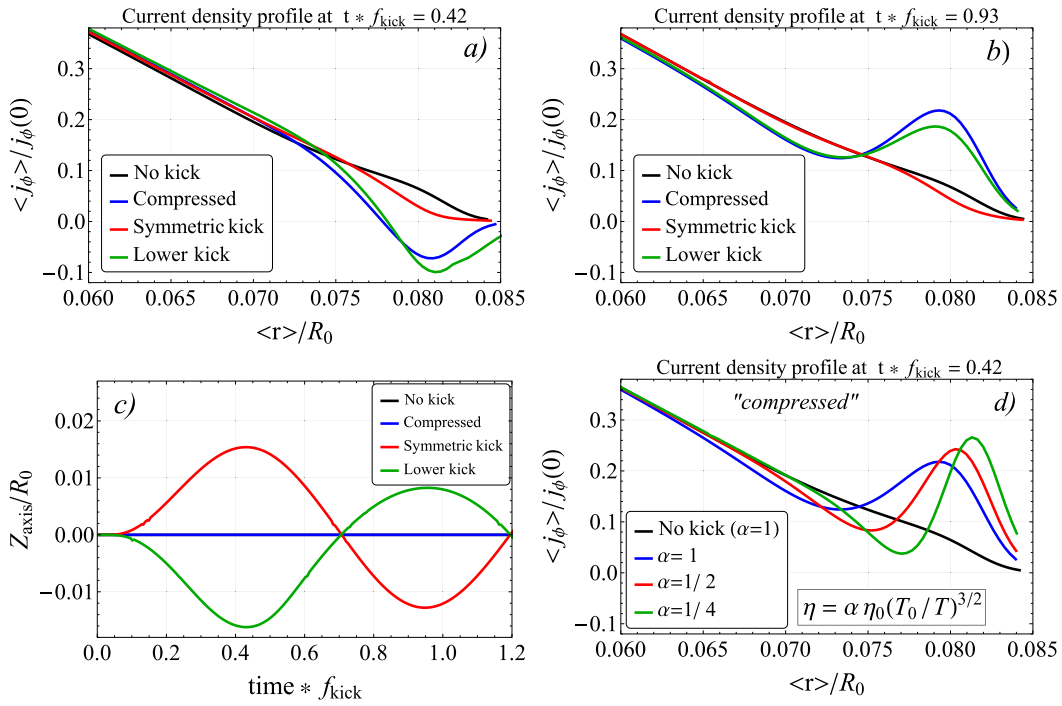

Figure 2. Current induction during vertical position oscillations for the symmetric PF coil configuration. (*a*) Averaged toroidal current density as a function of the averaged minor radius at time $\bar{t} = tf_{\rm kick} = 0.42$, (*b*) same for time $\bar{t} = tf_{\rm kick} = 0.93$. (*c*) Vertical position of the magnetic axis as a function of time. (*d*) Averaged toroidal current as a function of minor radius at time $\bar{t} = tf_{\rm kick} = 0.93$ for different plasma resistivities. Note that α is a scaling factor for the resistivity profile. The legends are explained in detail in section 2.1.1.

with equal sign and magnitude. The VS coil currents are sinusoidally varied over time with a frequency f for 3 different current waveforms

1. **'Compressed'**: The coil currents try to compress or expand the plasma as they share equal magnitude and sign. $I_{\rm VS1} = I_{\rm VS2} = I_0 \sin(2\pi ft)$. No vertical motion is expected.
2. **'Symmetric kick'**: Currents have equal magnitude but different signs. $I_{\rm VS1} = -I_{\rm VS2} = I_0 \sin(2\pi ft)$. Vertical motion is expected.
3. **'Lower coil kick'**: Only the lower coil is used. $I_{\rm VS1} = 0$ and $I_{\rm VS2} = 2 * I_0 \sin(2\pi ft)$. Vertical motion is expected with enhanced lower displacement.

In figure 2, we show the position of the plasma center over time together with the averaged[8] toroidal current profiles at the times when the plasma reaches its extreme positions. From this figure we observe that the impact of a symmetric oscillation on the edge current is not significant. However, only using the lower coil or using both coils with the same current sign induces a significant amount of negative edge current. This is in agreement with our previous analytical model (equation (6)) when considering the term $\delta\psi_{\rm ext}(a_0)$ which can drive current without plasma motion. Only the cases that produce net external flux $\delta\psi_{\rm ext}$ induce currents, the 'symmetric kick' case is the only one that does not produce net external flux because the fluxes produced by the VS coils with different sign and same magnitude cancel. A scan on the resistivity (η) is also performed for the 'compressed' case, which reveals that the penetration depth of the current increases with resistivity; this agrees quantitatively with the scaling of the skin depth $\delta_{\rm skin} \propto \sqrt{\eta}$. As shown in figure 2(*d*), increasing the resistivity by a factor 4 implies an increase of the penetration depth by a factor 2.

2.1.2. Asymmetric PF coils. The second configuration has a vertical asymmetry on the PF coils with respect to the magnetic axis (see figure 1(*b*)), which creates a lower *X*-point close to the plasma.

In figure 3 we show the induced current for the case of an oscillation with symmetry in the VS coils ('symmetric kick'). When moving upwards, a small positive current is induced, but when moving towards the near *X*-point a significant negative current is induced. Our analytical model can explain these results by considering the terms $\delta\mathbf{r}\cdot\nabla\psi_{\rm ext}$ and $-B_\theta(r_0)R_0\delta w_r$ of equation (6). The magnetic field gradient is larger in the lower position and therefore when the plasma approaches PF2 it experiences a net increase of external poloidal flux which drives a current by the term $\delta\mathbf{r}\cdot\nabla\psi_{PF2}$. The plasma also experiences an expansion as its lower part is more attracted by PF2 than the upper part. This enhances as well an additional decrease of current through the term $-B_\theta(r_0)R_0\delta w_r$. A more intuitive explanation for the negative sign is the fact that the plasma approaches a current with the same sign, and therefore a screening current with opposite sign is induced inside the plasma. From this point of view, we would generally expect to induce negative currents when the plasma moves towards the closest *X*-point. However, positive currents are induced in that situation for JET and ITER geometries. As it will be

[8] Quantities with $\langle\rangle$ are averaged on the flux surfaces contours. $\langle A\rangle \equiv \left(\oint_{\psi=\rm cte} A\mathrm{d}l\right) / \left(\oint_{\psi=\rm cte} \mathrm{d}l\right)$.

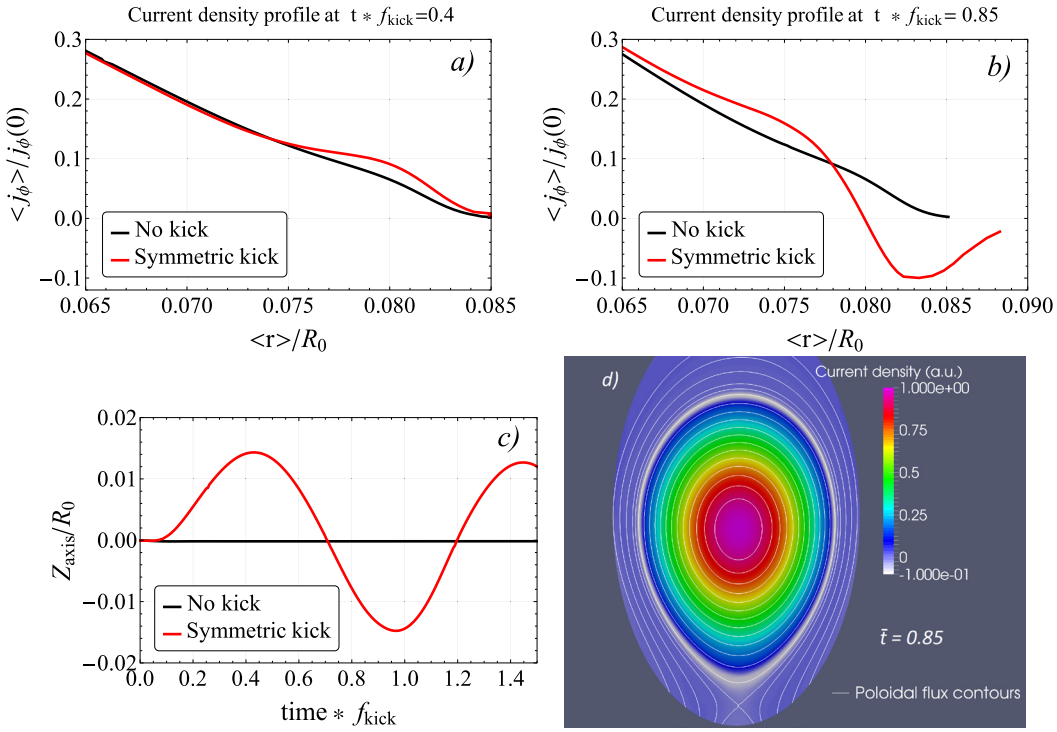

Figure 3. Current induction during vertical position oscillations for the asymmetric PF coil configuration. (*a*) Averaged toroidal current density as a function of the averaged minor radius for time $\bar{t} = tf_{kick} = 0.4$ at highest vertical position, (*b*) same for time $\bar{t} = tf_{kick} = 0.85$ at lowest position. (*c*) Vertical position of the magnetic axis as a function of time. (*d*) 2D contour map of the current density profile showing that the negative induced current is poloidally distributed along the flux surfaces at $\bar{t} = tf_{kick} = 0.85$.

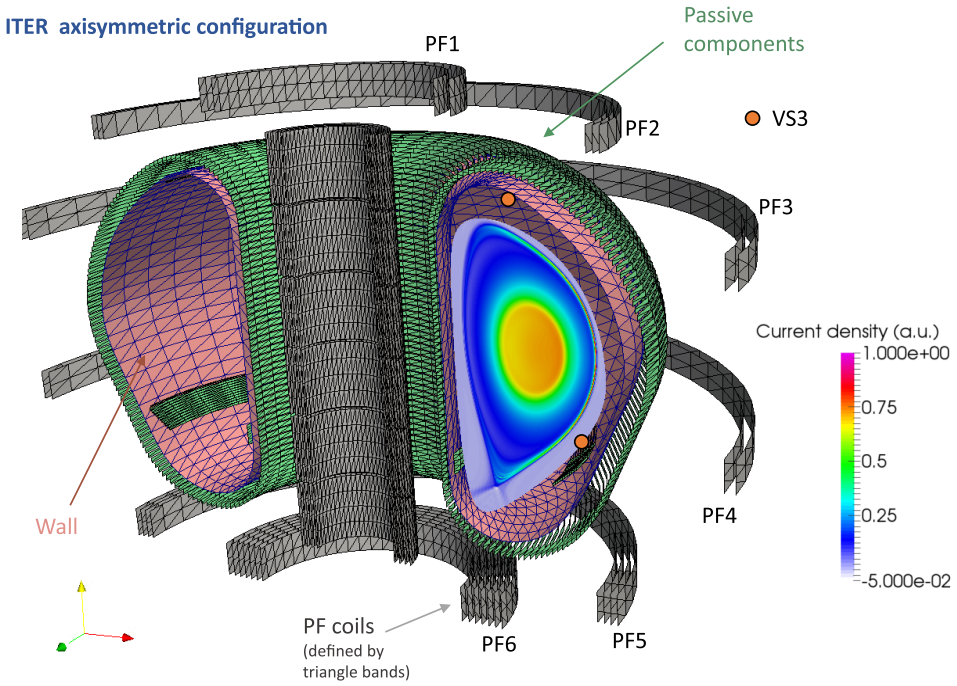

Figure 4. Geometrical modelling of PF coils, walls and passive structures in JOREK-STARWALL for the ITER case presented in [6].

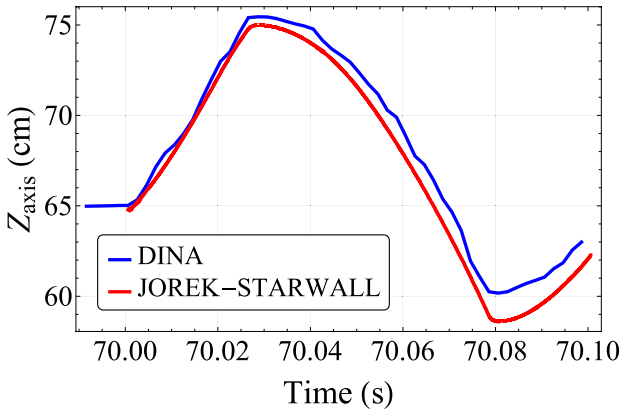

Figure 5. Benchmark of JOREK-STARWALL with the DINA case. The vertical position of the magnetic axis is shown over time during the vertical oscillation.

shown in the next section, ITER plasmas experience a reduction of volume in the latter case, which is the main cause of the increase in positive current.

2.2. ITER case

Here we perform an analysis of a realistic vertical position oscillation with a 7.5 MA/2.65 T ITER H-mode plasma. This case was presented in [6] for vertical oscillation studies with the code DINA and we have used it to benchmark JOREK-STARWALL. For the benchmark we have included the same 2D axisymmetric model for the ITER wall and passive structures, which STARWALL discretises in thin triangles (see figure 4). The vacuum vessel is modelled as two thin stainless steel layers with a width of 6 cm each, the conducting OTS (outer triangular support) and DIR (divertor inboard rail) are included as well.

We show the agreement of the plasma vertical position over time between JOREK-STARWALL and DINA in figure 5. It is important to note that in order to get this good agreement between the two codes we had to carefully implement all the mutual inductances of the system, in particular the mutual inductance between passive components and coils was required, otherwise the plasma final displacement obtained for a given set of currents could be overestimated by a factor of 2. This is due to the fact that the coils used to produce the vertical motion (VS3 in figure 4) are very close to the vacuum vessel and the triangular support, which can screen significantly the poloidal field created by the coils. We emphasize the fact that no ad hoc assumptions were done for the calculation of the inductances. All the mutual inductances of every single triangle with all the other existing triangles representing the various conductors, are numerically computed according to [10].

The vertical oscillation frequency for the benchmark case was $f = 10$ Hz and the total current variation in the in-vessel coils (VS3 system) was $\Delta I_{VS3} = 240$ kA-turns which is the maximum achievable with the VS3 coil design in ITER. In the following simulations, we have added two extra PF coils (AUX-1, AUX-2) in order to study the influence of different coil configurations on the induction of edge current during the vertical oscillation (see figures 6 and 7). The MHD model used for these simulations [12] includes parallel flows, Bohm boundary conditions and free outflow of density and temperature at the divertor plates. As an additional boundary condition, there is no current flow into the divertor targets. The plasma grid is aligned with the initial flux surfaces and the number of used Bezier elements is 24 464, mesh accumulation is used as well at the pedestal and at the *X*-point. The pedestal gradients are maintained due to a local reduction of the density and temperature diffusivities ($D_{\perp \mathrm{ped}} = 0.2 \times D_{\perp \mathrm{core}} = 4\ \mathrm{m^2\ s^{-1}}$, $\chi_{\perp \mathrm{ped}} = 0.1 \times \chi_{\perp \mathrm{core}} = 2\ \mathrm{m^2\ s^{-1}}$). The parallel heat diffusivity and kinematic viscosity at the core are respectively $\chi_{\parallel \mathrm{core}} = 8.4 \times 10^9\ \mathrm{m^2\ s^{-1}}$ and $\nu_{\parallel \mathrm{core}} = 20 \times \nu_{\perp \mathrm{core}} = 40\ \mathrm{m^2\ s^{-1}}$. Where the latter quantities have the following temperature dependences $\chi_\parallel \propto T^{5/2}$ and $\nu_\parallel \propto T^{-3/2}$. Note that the closure for the parallel heat flux assumes that the pedestal plasma is collisional, which is not the case. The investigation of more appropriate integral closures for the calculation of the parallel heat flux [13] is left for future work, although the chosen closure is not expected to have a mayor impact on the profiles before the ELM crash phase, which is the subject of our study.

Because of numerical stability related to the non-linear MHD ELM triggering simulations to be discussed in section 3, we have increased the plasma and wall resistivities by a factor of 15 as well as the oscillation frequency ($f_{\mathrm{new}} = 150$ Hz) keeping constant the ratio $\tau_{\mathrm{kick}}/\tau_\eta$ so that edge current induction in these simulations is representative of ITER plasmas. Thus the pedestal top resistivity corresponds to the Spitzer value for a temperature of 430 eV, which corresponds to a real plasma temperature of ~2.5 keV (when $f = 10$ Hz) as expected for 7.5 MA/2.65 T H-modes.

We have divided the results of the study into two figures (figures 6 and 7), where we show the different PF coil geometries, the used PF coil currents and the obtained time traces of different plasma quantities. The separatrix at time $t^* = 26$ ms[9] is also compared for the different configurations. The legend tables indicate the maximum total current used in the VS3 and AUX coils for the different cases. Note that currents larger than 240 kA-turns in any of the VS3 coils is beyond the ITER design limits, these values are only used to explore a wider range of the induced currents with an ITER-like geometry. Similarly the AUX coils do not exist in the ITER design and they are only used for understanding how edge currents are induced. Note that there is a special time trace (dark blue), where we have increased the wall resistivity by a further factor of 10 such that a natural VDE was destabilised. For that case, the chosen wall resistivity was such that the the plasma moved downwards with a similar time scale and displacement as the oscillation cases; this case allows us to study the current induction without the influence of time-varying coil currents.

The cases where more current I_{ped} is induced are the cases in which the plasma develops a larger reduction of the pedestal cross-sectional area A_{ped} (see figures 6(*b*) and 7(*b*)). It should be noted that some coil configurations are more efficient than others in reducing the plasma cross-section and thus inducing current. For example to use only the upper VS3 coil (green

[9] For clarity, we define the re-scaled time as $t^* \equiv 15 \times t_{\mathrm{simulated}}$.

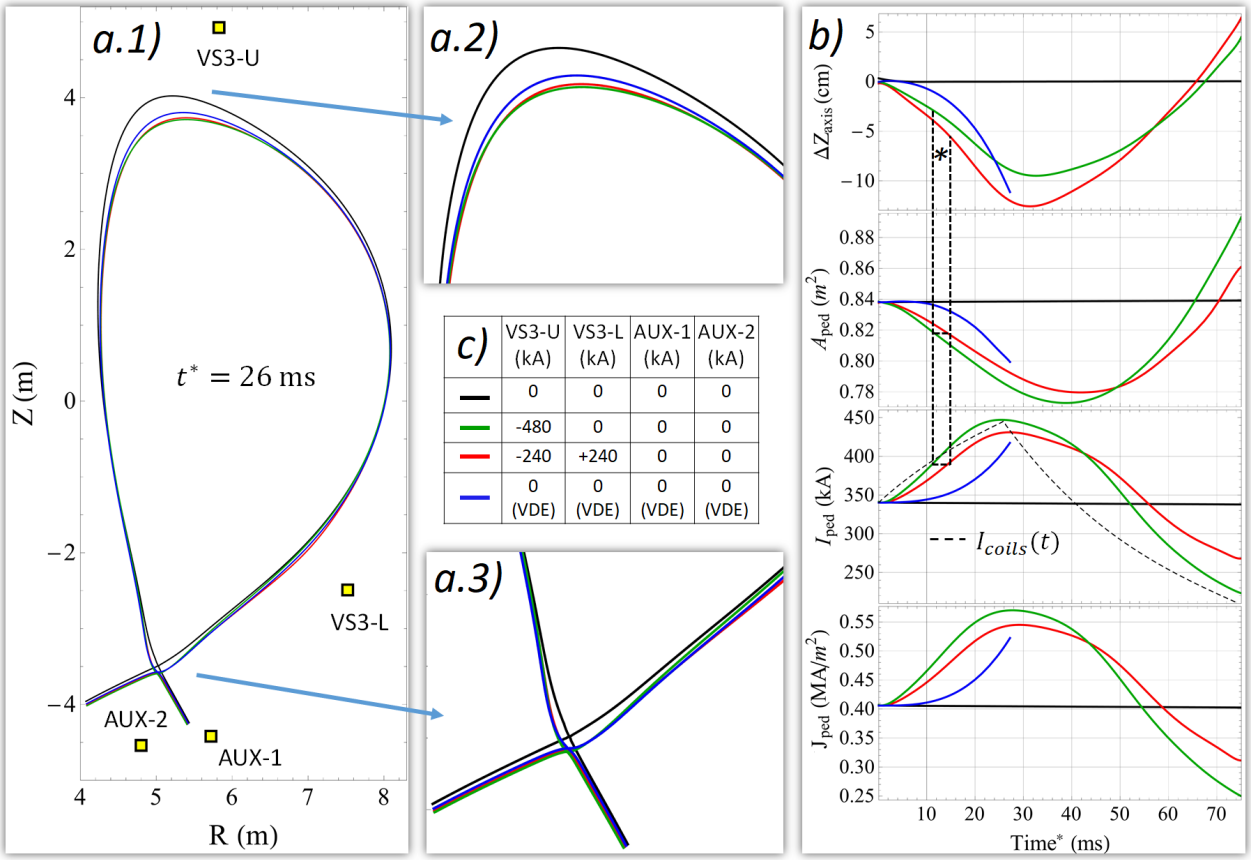

Figure 6. ITER current induction study for different coil configurations. (*a*) Separatrix at $t^* = 26$ ms for different coil currents and geometries. (*b*) Time traces of the vertical displacement of the magnetic axis ΔZ_{axis}, the pedestal area A_{ped}, the pedestal toroidal current I_{ped} and the averaged toroidal current density $J_{ped} \equiv I_{ped}/A_{ped}$. (*c*) Maximum current used (in kA-turns) in the time-varying coils for the different cases. Note that currents larger than 240 kA-turns in any of the VS3 coils is beyond the ITER design limits, these values are only used to extract physics results. Note as well that the AUX coils do not exist in the ITER design and are only used for physical understanding.

curve in figure 6) is more efficient than to use the two ITER VS3 coils in anti-series (red curve in figure 6) as required for vertical plasma stabilization. In order to obtain the same $I_{ped} = 390$ kA, using the VS3 coils in anti-series requires a vertical displacement of $\Delta Z_{axis} = 5.5$ cm while only using the upper VS3 coil requires $\Delta Z_{axis} = 3$ cm (see figure 6(*b*)*). The compression can be also enhanced by moving the position of the *X*-point with the AUX coils (see green curve in figure 7).

The VDE case is very similar to the case in which both VS3 coils are used in anti-series in terms of current induction, comparable currents are induced at similar positions and pedestal areas (see figure 6(*b*)). From this observation it can be concluded that the time-varying coil currents do not directly influence the pedestal current, but it is rather the resulting plasma motion that causes the compression and induces current. Therefore the term $\delta\psi_{ext,coils}(a_0)$ of equation (6) has little impact in this case. If that term were the dominant one, the case where the plasma position has been kept fixed and the coil currents aim to compress the plasma would have induced a significant current (see red curve of figure 7).

The change in plasma cross section is due to the fact that the top of the plasma (see figure 6(*a*.2)) moves faster than the *X*-point (see figure 6(*a*.3)). This effect is due to the vertical asymmetry of the external magnetic field produced by the PF coils. Therefore we expect a weaker induction of current for symmetric double-null plasmas. In figure 8 we show the change in external flux along the poloidal angle θ for the flux surface $\psi_N = 0.98$[10], the flux difference is taken after a downward displacement of $\Delta Z_{axis} = -1.4$ cm. The change in total external flux (blue curve) is separated into the contributions due to the currents in the walls and passive structures, the currents in the VS3 coils and the motion through the static field produced by the PF coils (motional effect). The figure reveals that total change in external flux ($\delta\psi_{ext}$) is determined by the motional effect contribution ($\delta\mathbf{r}\cdot\nabla\psi_{PF}$) while the other contributions cancel approximately each other.

As an overall conclusion, the increase in pedestal current arises from the motion of the plasma through the asymmetric magnetic field produced by the PF coils in ITER single-null plasmas. During the vertical motion, the reduction of plasma cross-section and the variation of external flux cause an increase of current through the terms $-B_\theta(r_0)R_0\delta w_r$ and $\delta\mathbf{r}\cdot\nabla\psi_{PF}$ of equation (6). Plasma compression can be enhanced by using different coil configurations to move the plasma as well.

[10] The radial coordinate ψ_N is the normalized poloidal flux, being 1 at the separatrix and 0 at the plasma core.

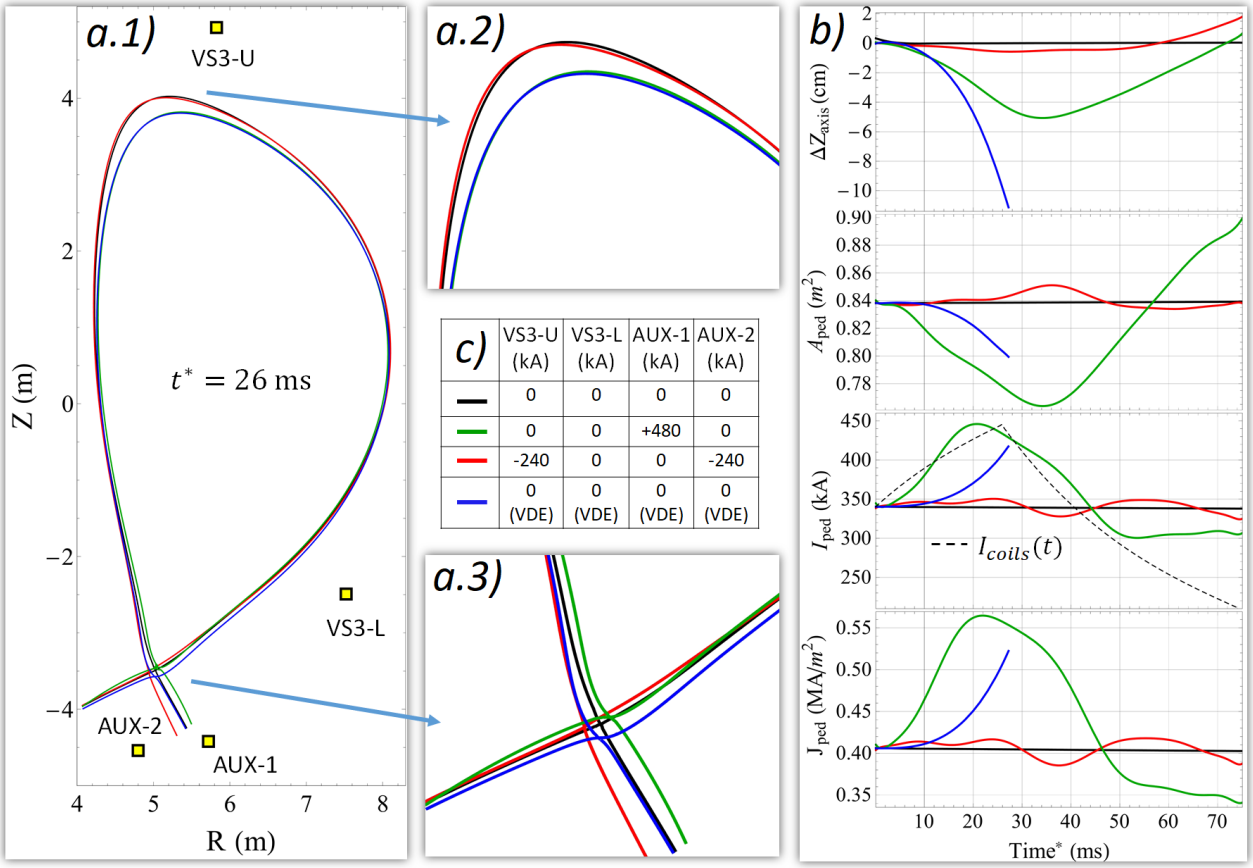

Figure 7. ITER current induction study for different coil configurations. (*a*) Separatrix at $t^* = 26$ ms for different coil currents and geometries. (*b*) Time traces of the vertical displacement of the magnetic axis ΔZ_{axis}, the pedestal area A_{ped}, the pedestal toroidal current I_{ped} and the averaged toroidal current density $J_{ped} \equiv I_{ped}/A_{ped}$. (*c*) Maximum current used (in kA-turns) in the time-varying coils for the different cases. Note that currents larger than 240 kA-turns in any of the VS3 coils is beyond the ITER design limits, these values are only used to extract physics results. Note as well that the AUX coils do not exist in the ITER design and are only used for physical understanding.

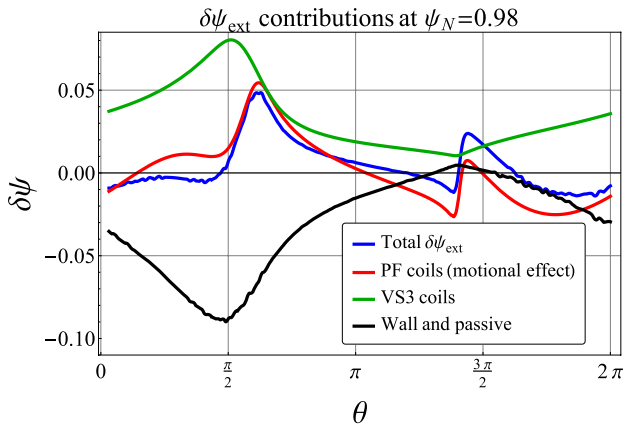

Figure 8. External flux variation at the $\psi_N = 0.98$ flux surface after a downward displacement of -1.4 cm. θ is the angle along the flux poloidal contour and the curves represent the different contributions to $\delta\psi_{ext}$. This case corresponds to the oscillation with $I_{VS3L} = -I_{VS3U} = 240$ kA. The flux difference is done with a small ΔZ in order to keep the plasma deformation small so the angle θ still identifies correctly the displaced position.

Finally the time traces also show that the change in the averaged current density δJ_{ped} is dominated by the change in total current $\delta I_{ped}/I_{ped} \sim 23\%$ rather than the change in the pedestal area $\delta A_{ped}/A_{ped} \sim 8\%$.

3. ELM triggering for an ITER plasma

In this section we study the non-linear MHD stability of ITER plasmas subjected to vertical position oscillations as described in the previous section. As a reminder, the frequency of the vertical motion was scaled by a factor 15 ($f = 10 \rightarrow 150$ Hz) as well as the wall and plasma resistivities in order to keep the ratio τ_{kick}/τ_η constant. Unless noted otherwise, the vertical oscillation is performed with the ITER baseline coil configuration (VS3 U/L) with maximum current amplitudes of 240 kA-turns per coil. As our main interest is to show the ELM destabilization principle, we only consider the toroidal mode number $n = 6$ interacting non-linearly with the axisymmetric mode $n = 0$ for the sake of simplicity. More realistic simulations would require to include diamagnetic and neoclassical

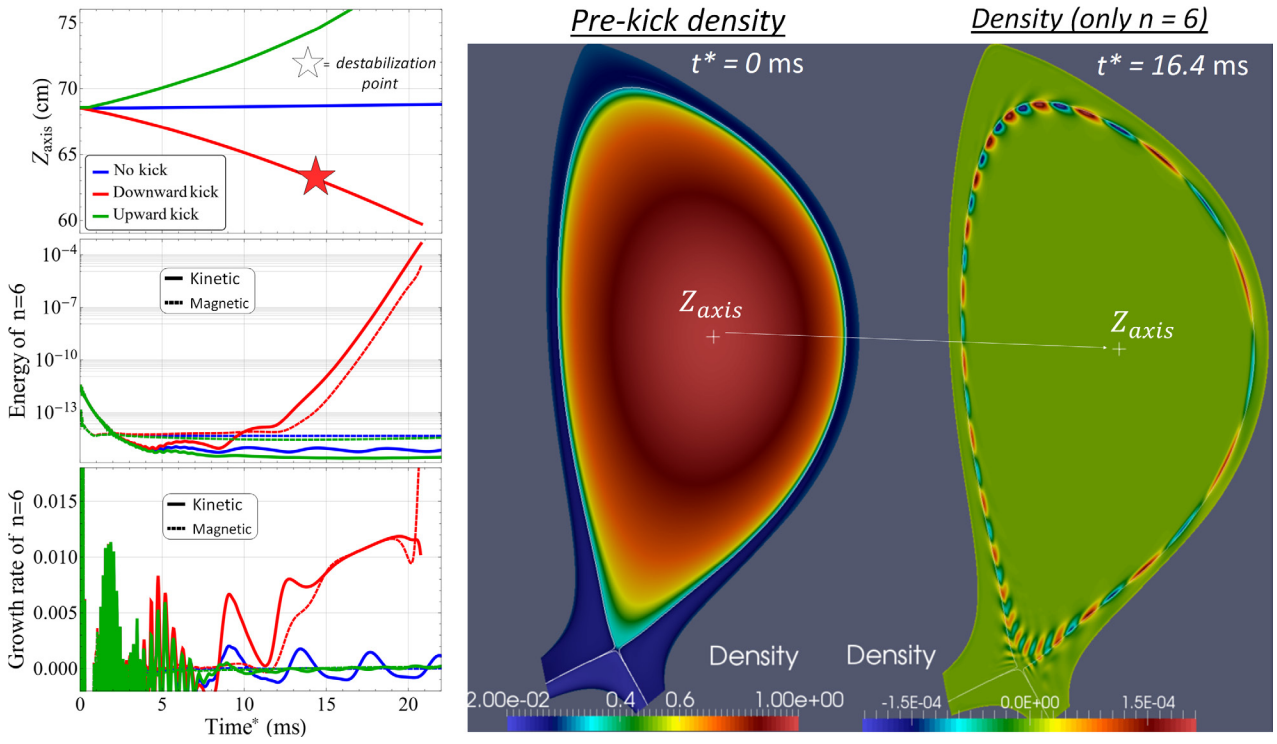

Figure 9. (Left) time traces of the position of the magnetic axis, the normalized energies and growth rates of the mode $n = 6$. (Right) pre-kick plasma density and the destabilized $n = 6$ linear mode structure of the density.

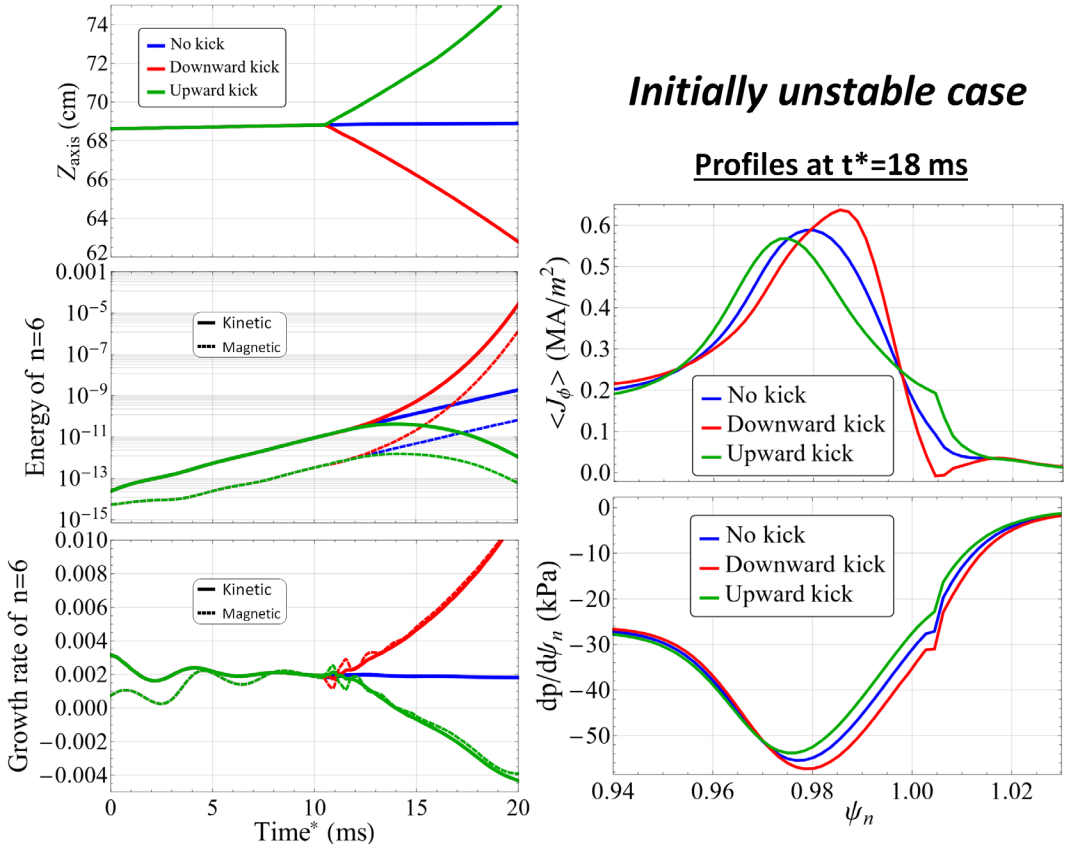

Figure 10. (Left) time traces of the position of the magnetic axis, the normalized energies and growth rates of the mode $n = 6$. (Right) averaged toroidal current and pressure gradient profiles at $t^* = 18$ ms. For this particular case, the time-scale of the motion τ_{kick} has been reduced by a factor 2 to better observe the change in the growth rates before reaching the non-linear phase of the downward kick case.

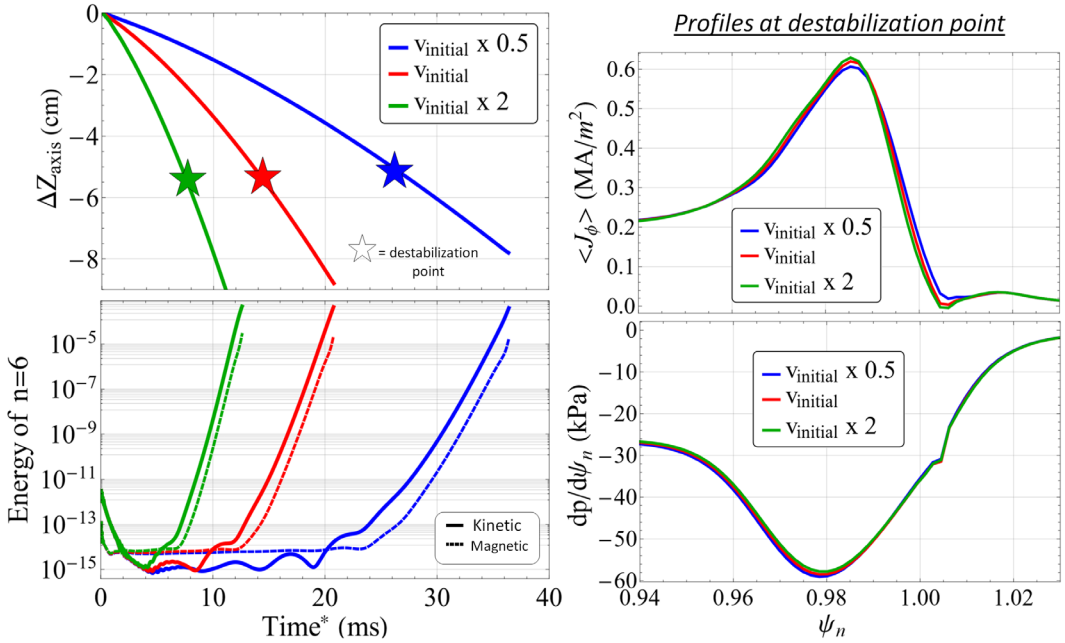

Figure 11. (Left) time traces of the position of the magnetic axis and the normalized energies of the mode $n = 6$. (Right) averaged toroidal current and pressure gradient profiles at the destabilization point.

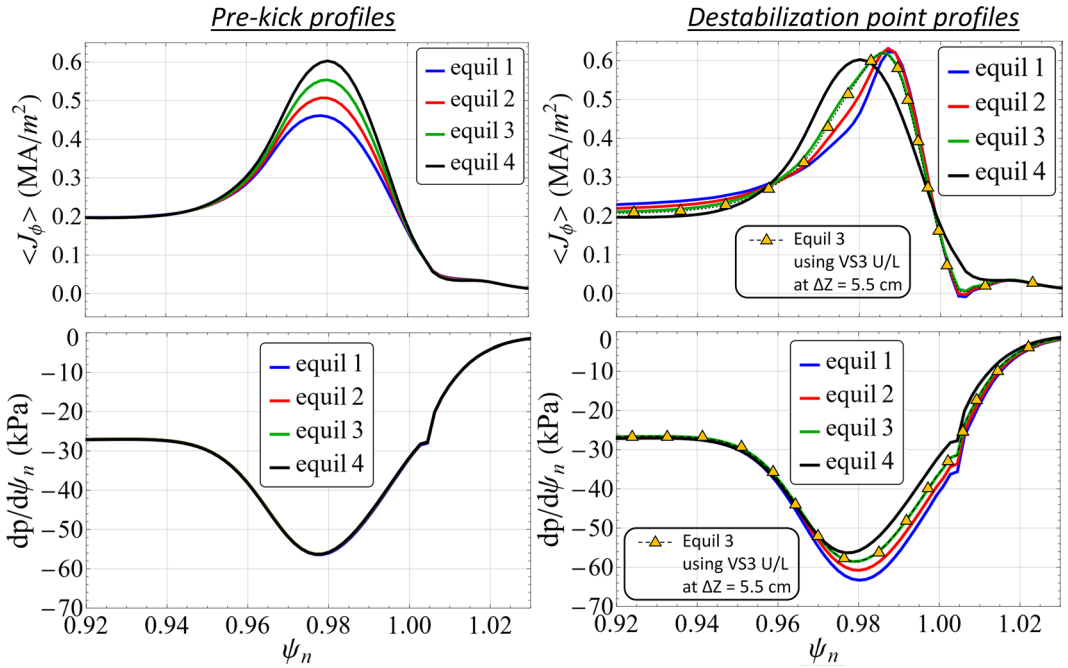

Figure 12. Profiles for the vertical oscillation shown in (figure 13). (Left) initial current and pressure profiles. (Right) profiles at the destabilization points. For reference, the dashed curve indicates the profiles at the destabilization point when using the baseline coil configuration (see figure 9), where the starting equilibrium corresponds to the green curve.

flows in our model in order to stabilize high-n mode numbers; we leave this task for future work.

In figure 9 we present an example of how an initially stable $n = 6$ mode can be destabilized by applying a vertical downward motion. The destabilized mode structure presents the characteristics of a peeling–ballooning mode [7] formed close to the plasma separatrix. We define the destabilization point as the time in which the magnetic and kinetic growth rates agree within 10% and a mode structure is clearly formed. An upward vertical motion was also applied but this does not lead to the increase of the plasma kinetic and magnetic energies nor to the triggering of an ELM. In order to study in more detail the effect of upward and downward motions, we repeat the same study for an initially unstable case and we analyse its influence on the growth rate.

The study shown in figure 10 reveals that a downward motion can further destabilize an initially unstable peeling–ballooning mode by increasing its growth rate. On the other hand, the upward motion can decrease the growth rate down to negative values and stabilize the mode. A comparison

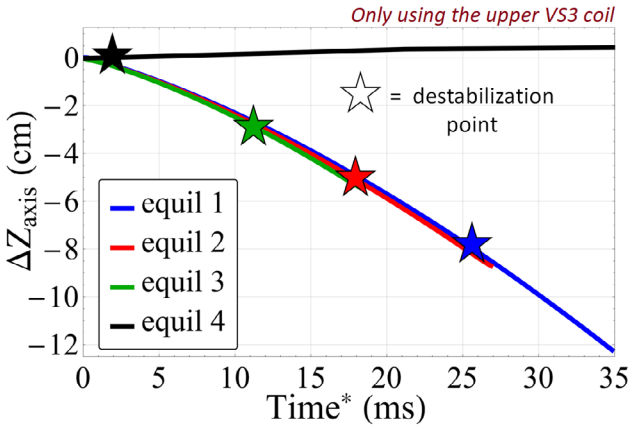

Figure 13. Plasma vertical displacement with time for the different starting equilibria (figure 12). The destabilization points are marked with a star symbol.

of the current and pressure gradient profiles at points with increasing, constant and decreasing growth rate shows that the destabilizing mechanism can be associated with changes in the pedestal current. Indeed increasing the current density at the pedestal and at the separatrix drives the peeling–ballooning modes more unstable. It is also important to note that in these simulations the edge pressure gradient increases during the downward motion and this could be an additional destabilization mechanism for the ELM.

Experiments in JET [3] demonstrated that the triggering of ELMs by vertical plasma oscillations strongly depends on the plasma displacement ΔZ_{axis} but not on the plasma velocity during the oscillation. In figure 11 we show the results of a scan on the plasma vertical velocity for a downward motion. For an initially stable case, an ELM was destabilized at the same vertical displacement ($\Delta Z_{axis} \approx 5.5$ cm) for the the three cases with different velocities of the vertical motion in agreement with experimental observations. If we assume that the induced edge current is the main cause of the ELM destabilization, this could be well explained by the prediction of equation (6), where the plasma speed only plays a role through the resistive decay term (which is expected to be very small for the high pedestal plasmas in ITER H-modes). At the destabilization point, the current and pressure gradient profiles were very similar, supporting the idea that the ELM triggering can be described in terms of the stability of equilibrium states, i.e. it does not depend on the kick velocity.

In order to further explore the influence of the induced edge current on the triggering of ELMs, we have performed the same vertical position oscillation on four different starting equilibria. For this vertical oscillation study only the upper VS3 coil has been used as this coil configuration induces more current for smaller displacements and makes these physics target simulations possible[11]. The different starting equilibria have the same pressure profile but different averaged current profiles (figure 12 'pre-kick profiles'). If the instability is triggered by an increase of edge current during the vertical motion, we expect to require bigger displacements for lower initial edge currents. Indeed, the results shown in figure 13 support this hypothesis. Moreover, the destabilization occurs when the current density values become comparable to the initially unstable case, i.e. the black curve. As it can be observed, the pressure profiles also vary during the motion, this is due to the adiabatic compression of the pedestal that follows the law $PV^{\gamma} = \text{cte}$. Therefore the evolution of the pressure profile could potentially contribute to the triggering of the ELM instability. However this effect cannot be the dominant one, as the starting pressure profiles were identical in all the cases and they present different peak values at the destabilization points which shows that the main destabilizing factor is the edge current. In addition the mode structure has a strong peeling component (figure 9) which reinforces the idea of the current as the main mechanism that destabilizes the ELM.

4. Conclusions

ELM triggering via vertical position oscillations has been experimentally demonstrated in the TCV [1], AUG [2] and JET [3] tokamaks proving to be a reliable technique for the ELM frequency control. In this paper, the physics of the ELM triggering mechanism via vertical oscillations was studied for the first time in non-linear MHD simulations with the free-boundary code JOREK-STARWALL and applied to ITER 7.5 MA/2.65 T H-mode plasmas.

References de la Luna *et al* and Gribov *et al* [3, 6] propose the induction of edge current during the vertical oscillation to trigger ELMs by this scheme. In this paper, a simple analytical model was derived in order to illustrate the origin of this current (equation (6)), showing it to be independent on the speed of the vertical motion for ideal plasmas and to result from a change on the boundary external flux and plasma compression. The edge current induction was also studied with JOREK-STARWALL for a simple elongated plasma and for a realistic ITER 7.5 MA/2.65 T H-mode plasma. For the simple case, the analysis showed that the induced current can be understood as a screening current reaction of the plasma against the change of external magnetic flux, either if the change is produced by a strong asymmetry in the VS coils ($\delta\psi_{VS}(a_0)$) or by the plasma motion through an inhomogeneous magnetic field ($\delta\mathbf{r}\cdot\nabla\psi_{PF}$). The ITER case revealed that the induced edge current can also be strongly related to the plasma compression due to its motion through the top-down asymmetric magnetic field. In addition, the results in figures 6 and 7 indicate that the compression and the induced current can be enhanced by choosing different geometries and current waveforms for the coils used to displace the plasma as already considered in [14].

The phenomenology of the non-linear MHD ELM triggering via vertical position oscillations was simulated in a consistent dynamic scheme for the first time. An initially stable $n = 6$ mode was found to be destabilized by a downward

[11] For the equilibrium with lowest current, the use of both VS3 coils in anti-series would require a downward displacement of ∼16 cm which significantly modifies the plasma geometry at the divertor making it very difficult to model.

motion and to remain stable when applying an upward one (see figure 9). The destabilized mode has the structure of a peeling–ballooning mode with a dominant peeling component. Additional simulations with an initially unstable plasma (see in figure 10), revealed that the mode was stabilized by the upward motion and further destabilized by a downward one. JOREK-STARWALL simulations revealed that the pre-oscillation edge current profile determines the minimum plasma displacement required to destabilize ELMs, with larger displacements being required for lower pre-oscillation edge currents (see figure 13). In agreement with experiments, ELM triggering does not depend on the plasma velocity but on the plasma displacement ΔZ_{axis} (figure 11). For practical applications at ITER, the minimum vertical displacement that is required for ELM triggering will strongly depend on the edge current, which is expected to be large in ITER due to the low pedestal collisionalities of H-mode plasmas. In the H-mode 7.5 MA/2.65 T plasma modelled, ELMs were triggered for displacements of 5–6 cm, these displacements can be obtained with the ITER VS3 coil set in anti-series for typical oscillation frequencies of 10–15 Hz and maximum currents of $I_{\text{VS3}} = 160$–200 kA-turns [6].

The simulations confirm the hypothesis of the induced edge current as the essential mechanism for the ELM destabilization. The requirement of larger displacements for lower initial currents and the fact that the edge current increases for downward motions reinforce the idea of the edge current as the main destabilizing factor. The destabilized mode presents a strong peeling structure as well. This mechanism can also explain the weak dependence of the ELM triggering on the vertical speed as indicated by equation (6). The role of pressure profile modifications during the vertical plasma oscillation do not seem to be the main driver for ELM triggering. However, an accurate assessment of the effects of the pressure gradient changes on the ELM triggering by vertical position oscillations requires further investigations.

Acknowledgment

The authors acknowledge access to the EUROfusion High Performance Computer (Marconi-Fusion) through EUROfusion funding.

Disclaimer

ITER is the nuclear facility INB no. 174. The views and opinions expressed herein do not necessarily reflect those of the ITER Organization.

References

[1] Degeling A., Martin Y., Lister J., Villard L., Dokouka V., Lukash V. and Khayrutdinov R. 2003 Magnetic triggering of ELMs in TCV *Plasma Phys. Control. Fusion* **45** 1637
[2] Lang P. *et al* 2004 Frequency control of type-i ELMs by magnetic triggering in asdex upgrade *Plasma Phys. Control. Fusion* **46** L31
[3] de la Luna E. *et al* 2015 Understanding the physics of ELM pacing via vertical kicks in jet in view of iter *Nucl. Fusion* **56** 026001
[4] Hölzl M., Merkel P., Huysmans G., Nardon E., Strumberger E., McAdams R., Chapman I., Günter S. and Lackner K. 2012 Coupling jorek and starwall codes for non-linear resistive-wall simulations *J. Phys.: Conf. Ser.* **401** 012010
[5] Loarte A. *et al* 2014 Progress on the application of ELM control schemes to ITER scenarios from the non-active phase to DT operation *Nucl. Fusion* **54** 033007
[6] Gribov Y., Kavin A., Lukash V., Khayrutdinov R., Huijsmans G., Loarte A., Snipes J. and Zabeo L. 2015 Plasma vertical stabilisation in iter *Nucl. Fusion* **55** 073021
[7] Huysmans G. 2005 Elms: MHD instabilities at the transport barrier *Plasma Phys. Control. Fusion* **47** B165
[8] Kim S. *et al* 2009 Comparing magnetic triggering of elms in tcv and asdex upgrade *Plasma Phys. Control. Fusion* **51** 055021
[9] Huysmans G. and Czarny O. 2007 MHD stability in x-point geometry: simulation of ELMs *Nucl. Fusion* **47** 659
[10] Merkel P. and Strumberger E. 2015 Linear MHD stability studies with the starwall code (arXiv:1508.04911)
[11] Jardin S. 2010 *Computational Methods in Plasma Physics* (Boca Raton, FL: CRC Press)
[12] Huysmans G., Pamela S., Van Der Plas E. and Ramet P. 2009 Non-linear mhd simulations of edge localized modes (ELMs) *Plasma Phys. Control. Fusion* **51** 124012
[13] Ji J.-Y., Yun G.S., Na Y.-S. and Held E.D. 2017 Electron parallel transport for arbitrary collisionality *Phys. Plasmas* **24** 112121
[14] Gribov Y., Kavin A., Lukash V., Khayrutdinov R., Huijsmans G. and Loarte A. 2015 Study of ELM triggering by axisymmetric in-vessel coils *42th EPS Conf. Plasma Physics* vol 39E p 125